Research on the Voltage Supporting Capability of Multi-VSC-HVDC Subsystems Operation Strategy to Receiving-end LCC-HVDC Network in Weak AC Grid

Tao Li, *Student Member*, *IEEE*, Yongli Li, *Senior Member*, *CES*, and Yuchen Zhu, *Student Member*, *IEEE*

***Abstract*—For the hybrid multi-infeed HVDC system in which the receiving-end grid is a strong AC grid including LCC-HVDC subsystems and multiple VSC-HVDC subsystems, it has higher voltage support capability. However, for weak AC grid, the voltage support capability of the multi-VSC-HVDC subsystems to the LCC-HVDC subsystem (voltage support capability-mVSCs-LCC) can resist the risk of commutation failure. Based on this consideration, this paper proposes an evaluation index called Dynamic Voltage Support Strength Factor (DVSF) for the hybrid multi-infeed system, and uses this index to qualitatively judge the voltage support capability-mVSCs-LCC in weak AC grid. In addition, the proposed evaluation index can also indirectly judge the ability of the LCC-HVDC subsystem to suppress commutation failure. Firstly, the mathematical model of the power flow of the LCC and VSC networks in the steady-state is analyzed, and the concept of DVSF applied to hybrid multi-infeed system is proposed. Furthermore, the DVSF index is also used to qualitatively judge the voltage support capability-mVSCs-LCC. Secondly, the influence of multiple VSC-HVDC subsystems with different operation strategies on the DVSF is analyzed with reference to the concept of DVSF. Finally, the indicators proposed in this paper are compared with other evaluation indicators through MATLAB simulation software to verify its effectiveness. More importantly, the effects of multi- VSC-HVDC subsystems using different coordinated control strategies on the voltage support capability of the receiving-end LCC-HVDC subsystem are also verified.**

***Index Terms*— Hybrid multi-infeed HVDC system, Voltage support, Multi-VSC-HVDC, LCC-HVDC, Commutation failure, DVSF, Control strategy.**

I. Introduction

LCC-HVDC has been widely used in traditional HVDC transmission projects because of its advantages in long-distance and large-capacity transmission [1]-[2], as shown in Fig.1 (a). However, the operation of the LCC-HVDC system has disadvantages such as relying on grid commutation, consuming more reactive power, and requiring a certain strength of AC grid. VSC-HVDC [3]-[5], as shown in Fig.1 (b), does not rely on AC system commutation, and can independently control active and reactive power. Following the trend, more and more VSC-HVDC will be fed into the load center, forming a pattern where LCC-HVDC and VSC-HVDC are mixed and fed into the grid [6]-[7], as shown in Fig.1 (c). When two types of HVDC systems are fed into the same AC grid, they will exhibit different operating characteristics from the single-infeed HVDC system. Therefore, it is of great theoretical and engineering significance to study the interaction between the two subsystems in the hybrid multi-infeed system, especially to quantitatively reflect and evaluate the voltage support capability -mVSCs-LCC in a weak AC grid.

To study the operating characteristics of the LCC-HVDC system, researchers have proposed a variety of evaluation indicators. Among them, the short-circuit ratio (SCR) [8-9] or effective SCR (ESCR) [10] of the AC system can be apply to quantitatively evaluate the strength of the HVDC system. Furthermore, commutation failure immunity index (CFII) [11] can reflect the ability of the LCC-HVDC system to suppress commutation failure. The above indicators are used to analyze the operating characteristics of the system when only LCC-HVDC is fed. When VSC-HVDC and LCC-HVDC form a hybrid multi-infeed HVDC system, the evaluation indicators need to be changed appropriately.

Regarding the impact of the VSC-HVDC subsystem on the LCC-HVDC subsystem in a multi-infeed system, researchers have carried out preliminary research and achieved certain results. Aiming at the problem that many previous ESCR

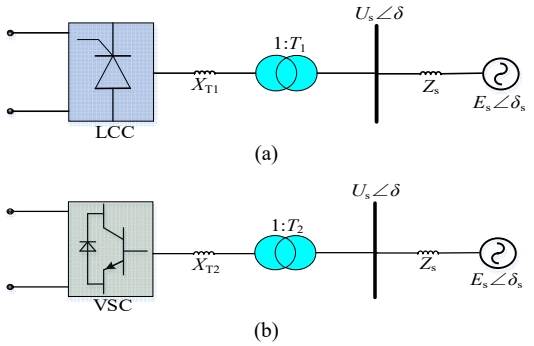

Manuscript received July 04, 2022; revised July 24, 2022; accepted 01, 2022. Date of publication March 25, 2023; Date of current version January 11, 2023.

This work was supported by the National Natural Science Foundation of China-State Grid Joint Fund for Smart Grid (No. U2066210).

T. Li, and Y. L. Li, and Y. C. Zhu are with the School of Electrical Automation and Information Engineering, Tianjin University, Tianjin, 300072, China (e-mail: litao_tju@sina.com; lyltju@163.com).

(Corresponding author: Yongli Li)

Digital Object Identifier 10.30941/CESTEMS.2023.00007

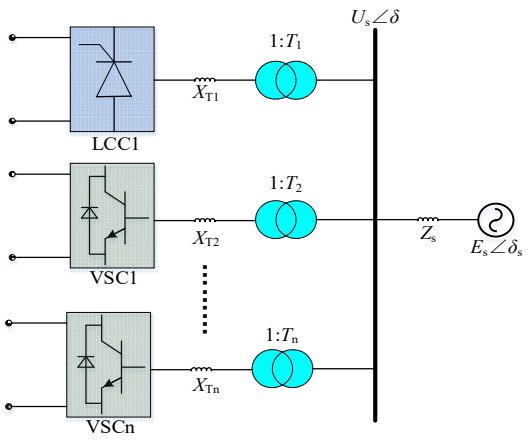

(c)

Fig. 1. Model in which the receiving-end HVDC transmission system uses different topological structures to feed into the same AC power grid. (a). single-infeed LCC-HVDC. (b). single-infeed VSC-HVDC. (c). hybrid multi-infeed HVDC.

calculation methods did not consider the operational impedance of the AC bus, *Aniruddha M. Gole*, *et al* [12] proposed an evaluation index called Impedance ESCR (IESCR). *Guo Chunyi*, *et al* [13] proposed an apparent increase in SCR (AISCR) index to discuss the effect of VSC-HVDC on the performance of LCC-HVDC. *Xiao Hao*, *et al* [14-15] used the concept of virtual impedance to equate the multi-infeed HVDC system to a single-infeed system, and proposed the unified ESCR (UESCR) to evaluate the strength of the equivalent HVDC system. The above method is derived from the concept of enhanced SCR to explore the effect of VSC-HVDC on LCC-HVDC, and simulations have verified the correctness of the proposed index. However, none of them considered the influence of multiple control strategies adopted by the VSC-HVDC subsystem on the LCC-HVDC subsystem. In particular, Ref.[12] only verified its effectiveness through simulation, and did not perform detailed theoretical calculations. Meanwhile, the equivalent impedance in Ref.[14], [15] needs to be obtained by complex power flow calculations, which undoubtedly increases the complexity of the evaluation index.

Some researchers also analyze the voltage support capability -mVSCs-LCC in the multi-infeed HVDC system from the power/voltage perspective. *Hau Aik, et al* [16] investigated the relationship between various voltage sensitivity and voltage interaction indicators from the perspectives of voltage, current, and power. Given the problem that the traditional multi-infeed interaction factor (MIIF) index only considers the influence of multi-infeed LCC-HVDC systems, *Xiao Hao*, *et al* [17] proposed an multi-infeed voltage interaction factor (MVIF) index to fully reflect the influence of the VSC-HVDC subsystem access on the LCC-HVDC. *Guo Chunyi*, *et al* [18] proposed a short-term voltage stability constraints (SVSCUC) index to explore the impact on the voltage support capability -mVSCs-LCC when the receiving-end LCC-HVDC system is disturbed. In view of the fact that there are multi-infeed HVDC subsystems in the receiving-end grid, *Hau Aik*, *et al* [19] proposed an Equivalent Nodal Voltage Sensitivity Factor (ENVSF) index to judge the voltage support capability -mVSCs-LCC. The above methods analyze the voltage support capability -mVSCs-LCC of the multi-infeed HVDC system from the perspective of voltage/power, and have certain theoretical and engineering reference significance. However, Ref.[16, 18] only considers the AC bus voltage support capability of multi-infeed LCC-HVDC system, and Ref.[17, 19] does not consider the influence of VSC-HVDC subsystem adopting multiple control strategies on the voltage support capability of LCC-HVDC subsystem.

Given the deficiencies of the above evaluation indicators, this paper proposes a new evaluation indicator called DVSF to quantitatively judge the voltage support capability -mVSCs-LCC in the hybrid multi-infeed HVDC system including the weak AC grid. Furthermore, this paper also analyzes in detail the influence of different control strategies adopted by the multi-VSC-HVDC subsystems on the voltage supporting capacity of the LCC-HVDC subsystem. Therefore, the core innovations of this paper and the reference role for the hybrid multi-infeed HVDC project to be constructed are as follows: (1) This paper presents an index that can evaluate the voltage support capability -mVSCs-LCC, which can qualitatively judge the ability of LCC-HVDC subsystem to suppress commutation failure in a hybrid multi-infeed system including the weak AC grid. (2) This paper also analyzes in detail the impact of the operation strategy of multiple VSC-HVDC subsystems on the voltage support capability -mVSCs-LCC of the hybrid three-infeed system, which can provide a certain reference for the operation mode of multiple VSC-HVDC subsystems in the hybrid DC project under construction or the traditional DC project to be reconstructed.

The remainder of this paper is organized as follows. Section II presents the system topology and steady-state power flow equations. The concept of dynamic voltage support strength factor (DVSF) is also proposed in this chapter. The impact of multiple VSC-HVDC subsystems with different control strategies on the LCC-HVDC subsystem is presented in Section III. Their assessment in simulation is presented in Section IV. Section V concludes.

II. The Concept of Dynamic Voltage Support Strength Factor

A. The Power Flow Equation in Steady-state

The schematic diagram of the hybrid multi-infeed network including one LCC-HVDC and two VSC-HVDCs is presented in Fig.2. As observed, ac systems are generally represented by system impedances $Z_s\angle\theta$ and equivalent electromotive force $E_s\angle\delta_s$. $U_s\angle\delta$ is the bus voltage with an AC filter. T_1, T_2, and T_3 are the transformation ratios of three transformers with equivalent reactances of X_{T1}, X_{T2}, and X_{T3}, respectively. I_{d1}, I_{d2} and I_{d3} are the DC-side currents of the three HVDC subsystems respectively. In the same way, U_{d1}, U_{d2} and U_{d3} are the DC-side voltages of the three HVDC subsystems at the receiving-end grid, respectively. P_{d1}, P_{d2} and P_{d3} are the active power flowing into the receiving-end grid from the three HVDC subsystems, respectively. Similarly, Q_{d1}, Q_{d2} and Q_{d3} are the corresponding reactive powers. P_s and Q_s are the active and reactive power of the equivalent system, and Q_c is the reactive power provided by the AC filter.

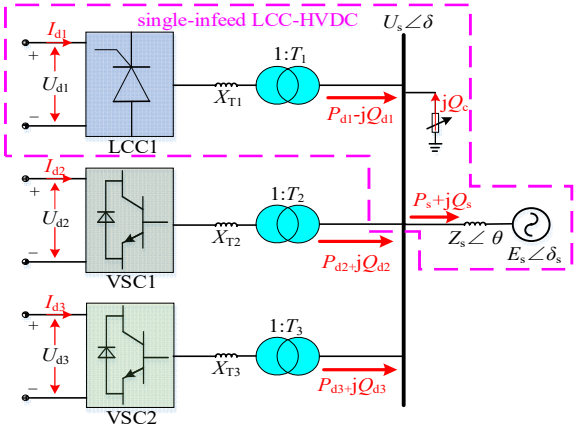

Fig .2. System model of the hybrid multi-infeed network including one LCC-HVDC and two VSC-HVDCs.

The steady-state power equation of the AC system is:

$$\begin{cases} P_s = \dfrac{R_s U_s^2 - U_s E_s (R_s \cos\delta - X_s \sin\delta)}{Z_s^2} \\ Q_s = \dfrac{X_s U_s^2 - U_s E_s (R_s \sin\delta + X_s \cos\delta)}{Z_s^2} \end{cases} \tag{1}$$

Where: Z_s=R_s+jX_s. Among them, R_s and X_s are the resistance and reactance of the AC grid, respectively.

When the LCC-HVDC subsystem uses constant DC current control (rectifier side) / constant extinction angle control (inverter side), the mathematical model is as follows:

$$\begin{cases} U_{d10} = \dfrac{6\sqrt{2}}{\pi T_1} U_s \\ U_{d1} = \dfrac{6\sqrt{2}}{\pi T_1} U_s \cos\gamma - \dfrac{6}{\pi} X_{T1} I_{d1} \\ P_{d1} = I_{d1} U_{d1} \\ Q_{d1} = I_{d1} \sqrt{U_{d10}^2 - U_{d1}^2} \end{cases} \tag{2}$$

Where: U_{d10} is the DC voltage output by the sending-end LCC-HVDC subsystem, which satisfies the relationship in (2) [12]. γ is the extinction angle of the receiving-end LCC-HVDC subsystem.

Since the power equations of VSC1-HVDC and VSC2-HVDC are identical, take VSC1-HVDC as an example, and its power equation is as follows:

$$\begin{cases} P_{d2} = \dfrac{U_s U_c \sin(\delta_c - \delta)}{T_2 X_{T2}} \\ Q_{d2} = \dfrac{T_2 U_s U_c \cos(\delta_c - \delta) - U_s^2}{T_2^2 X_{T2}} \end{cases} \tag{3}$$

Where: U_c and δ_c are the amplitude and phase angle of the VSC converter station's output voltage, and have the following relationship:

$$\begin{cases} U_c = \dfrac{T_2 \sqrt{(P_{d2} X_{T2})^2 + (Q_{d2} X_{T2} + U_s / T_2)^2}}{U_s} \\ \delta_c = \arcsin\left(\dfrac{P_{d2} X_{T2} T_2}{U_s U_c}\right) + \delta \end{cases} \tag{4}$$

The reactive power emitted by the AC filter connected to the AC bus has the following relationship:

$$Q_c = B_c U_s^2 \tag{5}$$

Where: B_c is the equivalent compensation capacitance of AC filter.

In addition, when the system is operating in a steady state, the power at the converter bus is balanced, as shown below:

$$\begin{cases} P_s = P_{d1} + P_{d2} + P_{d3} \\ Q_s = -Q_{d1} + Q_{d2} + Q_{d3} + Q_c \end{cases} \tag{6}$$

B. DVSF for the Hybrid Multi-infeed HVDC System

According to the maximum power curve of the LCC-HVDC system illustrated in Fig.3 [16], when the single-infeed LCC-HVDC system in the pink area of Fig.2 operates at dP_{d1}/dI_{d1}=0, it reaches the maximum transmission power, indicating that the limit of power stability has been reached. Under this situation, the voltage support capability of the LCC-HVDC system just satisfies the steady-state operation at the rated operating point, which is also called the critical operating point. Furthermore, facts have proved that if the system operates below this rated operating point, it will be difficult to maintain stability. However, the above judgment on the critical stability of the voltage support capability does not consider the role of the VSC-HVDC subsystem. Therefore, this paper will explore the impact of the VSC-HVDC subsystem on the maximum power curve (dP_{d1}/dI_{d1}).

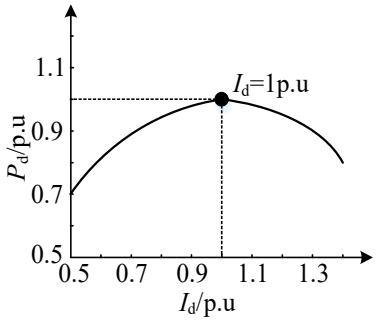

Fig. 3. Maximum power curve of HVDC system.

When there is external disturbance or power flow transfer between the receiving-end converter stations, the power balance at the converter bus may be temporarily broken. Let ΔP and ΔQ be the active power variable and the reactive power variable flowing into the grid from the converter bus, respectively. Then, from (6), we known that,

$$\begin{cases} \Delta P = \Delta P_s - \Delta P_{d1} - \Delta P_{d2} - \Delta P_{d3} \\ \Delta Q = \Delta Q_s + \Delta Q_{d1} - \Delta Q_{d2} - \Delta Q_{d3} - \Delta Q_c \end{cases} \tag{7}$$

Where: ΔP_s and ΔQ_s are the power variables of the AC system respectively. ΔP_{d1} and ΔQ_{d1} are the power variables of the LCC-HVDC subsystem respectively. In the same way, the physical meaning of ΔP_{d2}, ΔQ_{d2}, ΔP_{d3} and ΔQ_{d3} can be known. ΔQ_c is the reactive power variable provided by the AC filter.

In order to explore the voltage support capability -mVSCs-LCC, it is necessary to do disturbance analysis of the receiving-end AC network, let:

$$\Delta U_s = \frac{\partial U_s}{\partial Q} \Delta Q + \frac{\partial U_s}{\partial P} \Delta P \tag{8}$$

Where: $\partial U_s/\partial Q$ represents the sensitivity of the converter bus voltage to the injected reactive power when the active power remains unchanged. $\partial U_s/\partial P$ represents the sensitivity of the

converter bus voltage to the injected active power when the reactive power remains unchanged.

According to (2), when the single-infeed LCC-HVDC system adopts constant DC current control/constant extinction angle control, the power variation of the converter bus has the following relationship:

$$\begin{cases} \Delta P_{d1} = \dfrac{\partial P_{d1}}{\partial U_s}\Delta U_s + \dfrac{\partial P_{d1}}{\partial I_{d1}}\Delta I_{d1} \\ \Delta Q_{d1} = \dfrac{\partial Q_{d1}}{\partial U_s}\Delta U_s + \dfrac{\partial Q_{d1}}{\partial I_{d1}}\Delta I_{d1} \end{cases} \tag{9}$$

Simplified (9),

$$\frac{\Delta P_{d1}}{\Delta I_{d1}} = \frac{\partial P_{d1}}{\partial U_s}\left(\frac{\Delta Q_{d1}}{\Delta I_{d1}} - \frac{\partial Q_{d1}}{\partial I_{d1}}\right)\frac{\partial U_s}{\partial Q_{d1}} + \frac{\partial P_{d1}}{\partial I_{d1}} \tag{10}$$

Combining (8) and (9), yield:

$$\frac{\Delta Q_{d1}}{\Delta I_{d1}} = \frac{\dfrac{\partial U_s}{\partial P}\cdot\dfrac{\Delta P_{d1}}{\Delta I_{d1}} - \dfrac{\partial Q_{d1}}{\partial I_{d1}}\cdot\dfrac{\partial U_s}{\partial Q_{d1}}}{\dfrac{\partial U_s}{\partial Q} - \dfrac{\partial U_s}{\partial Q_{d1}}} \tag{11}$$

By substituting (11) into (10):

$$\frac{\Delta P_{d1}}{\Delta I_{d1}} = \frac{\dfrac{\partial P_{d1}}{\partial I_{d1}} - \dfrac{\partial P_{d1}}{\partial U_s}\cdot\dfrac{\dfrac{\partial Q_{d1}}{\partial I_{d1}}\cdot\dfrac{\partial U_s}{\partial Q_{d1}}}{\dfrac{\partial U_s}{\partial Q} - \dfrac{\partial U_s}{\partial Q_{d1}}} - \dfrac{\partial P_{d1}}{\partial U_s}\cdot\dfrac{\partial Q_{d1}}{\partial I_{d1}}\cdot\dfrac{\partial U_s}{\partial Q_{d1}}}{1 - \dfrac{\partial P_{d1}}{\partial U_s}\cdot\dfrac{\dfrac{\partial U_s}{\partial P}\cdot\dfrac{\partial U_s}{\partial Q_{d1}}}{\dfrac{\partial U_s}{\partial Q} - \dfrac{\partial U_s}{\partial Q_{d1}}}} \tag{12}$$

When $\Delta P_{d1}/\Delta I_{d1}=0$, the receiving-end LCC-HVDC system is in a stable state with a critical voltage, and there is the following relationship at this time:

$$\frac{\partial U_s}{\partial Q} = \frac{\partial U_s}{\partial Q_{d1}} + \frac{\dfrac{\partial Q_{d1}}{\partial I_{d1}}\cdot\dfrac{\partial U_s}{\partial Q_{d1}}\cdot\dfrac{\partial P_{d1}}{\partial U_s}}{\dfrac{\partial P_{d1}}{\partial I_{d1}} - \dfrac{\partial Q_{d1}}{\partial I_{d1}}\cdot\dfrac{\partial U_s}{\partial Q_{d1}}\cdot\dfrac{\partial P_{d1}}{\partial U_s}} \tag{13}$$

Where:

$$\begin{cases} \dfrac{\partial P_{d1}}{\partial U_s} = \dfrac{6\sqrt{2}}{\pi T_1} I_{d1}\cos\gamma \\ \dfrac{\partial P_{d1}}{\partial I_{d1}} = \dfrac{6\sqrt{2}}{\pi T_1} U_s\cos\gamma - \dfrac{12}{\pi} X_{T1} I_{d1} \\ \dfrac{\partial Q_{d1}}{\partial U_s} = \dfrac{6\sqrt{2} I_{d1}}{\pi T_1\sqrt{U_{d10}^{\ 2} - U_{d1}^{\ 2}}}(U_{d10} - U_{d1}\cos\gamma) \\ \dfrac{\partial Q_{d1}}{\partial I_{d1}} = \sqrt{U_{d10}^{\ 2} - U_{d1}^{\ 2}} + \dfrac{12 I_{d1} U_{d1} X_{T1}}{\pi\sqrt{U_{d10}^{\ 2} - U_{d1}^{\ 2}}} \end{cases} \tag{14}$$

When considering the impedance in AC system, the following relationship exists [20]:

$$\frac{\partial U_s}{\partial Q} = \frac{Z_s\sin\theta + \dfrac{Z_s^{\ 2}}{U_s^{\ 2}}Q}{U_s^{\ 3} - \dfrac{Z_s^{\ 2}}{U_s^{\ 3}}(P^2 + Q^2)} \tag{15}$$

Where: θ is the impedance angle of the AC system.

The voltage support capability of the LCC-HVDC subsystem is affected by the difference in reactive power absorbed by the converter bus at the receiving-end. As a result, the concept of dynamic voltage support strength factor (DVSF) is created to meet the goal of dynamically reflecting the voltage stability of the converter bus when the reactive power injected into the receiving-end system changes:

$$\mathrm{DVSF} = \left.\frac{\Delta Q}{\Delta U_s}\right|_{\substack{I_d=1 \\ P_d=P_{dN},\, Q_d=Q_{dN},\ X_s}} \tag{16}$$

Where: I_d =1 means that the receiving-end LCC-HVDC subsystem adopts constant DC current control, P_{dN} and Q_{dN} represent the rated operating state of the receiving-end VSC-HVDC subsystem. X_s represents the known system impedance of the AC grid, and usually X_s = 1/2~1/3 in a weak AC system.

According to (13), (15), and TABLE I, the DVSF values for both cases in Fig.4 can be obtained. Among them, Fig.4(a) is the DVSF value under different extinction angles obtained according to (12). As observed, with the increase of γ, the value of DVSF continues to decrease. Especially when $\gamma = 24^0$ or 26^0, the value of DVSF basically does not change. Therefore, considering a certain margin of extinction angle, the corresponding DVSF value when $\gamma = 18^0$ is selected as the judgment of whether the system is operating normally, that is, DVSF=0.5229. When DVSF<0.5229, the LCC-HVDC subsystem will not operate, and it is also called the weakest LCC-HVDC system. In addition, it should be noted here that the DVSF value calculated according to (13) only considers the case where the receiving-end grid contains only a single LCC-HVDC subsystem, and does not consider the access of the VSC-HVDC subsystem. Therefore, the DVSF value at this time indicates that the voltage support capability of the LCC-HVDC subsystem is the weakest.

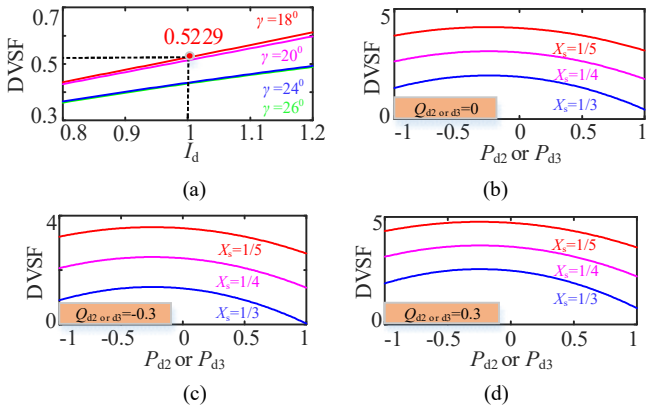

Fig. 4. The value of DVSF in two cases. (a).system impedance is not considered. (b). $Q_{d2\ or\ d3}$ = 0. (c). $Q_{d2\ or\ d3}$ = -0.3. (d). $Q_{d2\ or\ d3}$ = 0.3.

Similarly, Fig.4(b), Fig.4(c), and Fig.4(d) are the DVSF values under different system impedances obtained according to (15) when I_d=1. It should also be noted here that for the receiving-end grid only contains a single LCC-HVDC system, the value of the system impedance of the receiving-end grid determines the voltage support capability of the LCC-HVDC system, that is, the greater the short-circuit ratio (SCR) determined by the system impedance, the stronger the voltage

support capacity of the LCC-HVDC system [8-10]. However, when the receiving-end grid contains both the VSC-HVDC subsystem and the LCC-HVDC subsystem, the voltage support capability of the LCC-HVDC system is not only related to the system impedance but also to the operation strategy of the VSC-HVDC subsystem. Especially for a weak AC system, the coordinated control strategy adopted by the multi-VSC-HVDC subsystems is crucial for the LCC-HVDC subsystem. The simulation results in Fig.4(b), Fig.4(c) and Fig.4(d) are intended to illustrate this point. Observing them, with the decrease of system impedance, the value of DVSF shows an increasing trend. Meanwhile, Fig.4(b), Fig.4(c) and Fig.4(d) can clearly judge the influence of the output power of VSC-HVDC subsystem on the DVSF. Furthermore, as long as the rated state of VSC-HVDC subsystem is determined, the strength division standard of the LCC-HVDC system can be determined in weak AC grid.

In summary, the LCC-HVDC system strength judgment shown in (17) can be obtained. As observed, when DVSF<0.5229, the voltage support ability of the LCC-HVDC system is the weakest, indicating that the ability to suppress commutation failure is the lowest. When considering the access of the VSC-HVDC subsystem, the voltage support capability of the LCC-HVDC system is correspondingly improved, and its ability to suppress commutation failure is improved.

$$\begin{cases} DVSF < 0.5229, \text{weakest LCC-HVDC system} \\ 0.5229 < DVSF < \left.\dfrac{\Delta Q}{\Delta U_s}\right|_{\substack{I_d=1 \\ P_d=P_{dN},Q_d=Q_{dN},\ X_s=1/2\sim1/3}}, \text{ weak LCC-HVDC system} \\ DVSF > \left.\dfrac{\Delta Q}{\Delta U_s}\right|_{\substack{I_d=1 \\ P_d=P_{dN},Q_d=Q_{dN},\ X_s=1/2\sim1/3}}, \text{strong LCC-HVDC system} \end{cases} \tag{17}$$

III. THE IMPACT OF MUTI-VSC-HVDC SUBSYSTEMS USING DIFFERENT CONTROL STRATEGIES ON DVSF

It has been mentioned in the above chapters that the voltage support capability of the LCC-HVDC system in the hybrid multi-infeed network is related to the system impedance and the operation strategy of the VSC-HVDC subsystem. However, how the operation strategy of the VSC-HVDC subsystem affects the voltage support capability of the LCC-HVDC system needs further research. The following will explore the influence of different control strategies used by the VSC-HVDC subsystem on the DVSF. In addition, according to the future development plan of China Southern Power Grid, it will gradually build multiple VSC-HVDC networks on the receiving-end power grid based on the traditional LCC-HVDC project. Therefore, the content studied in this chapter has an important guiding role for the construction of future power grids.

According to (7), the power flow Jacobian matrix of the hybrid three-infeed HVDC transmission system can be established [15]:

$$\begin{bmatrix} \Delta P \\ \Delta Q \end{bmatrix} = \begin{bmatrix} J_{P\delta} & J_{PU} \\ J_{Q\delta} & J_{QU} \end{bmatrix} \begin{bmatrix} \Delta\delta \\ \Delta U_s / U_s \end{bmatrix} \tag{18}$$

Where: $J_{P\delta}$, J_{PU}, $J_{Q\delta}$ and J_{QU} are elements in the Jacobian matrix, and there are the following relationships:

$$\begin{cases} J_{P\delta} = \dfrac{\partial P}{\partial \delta}, \ J_{PU} = \dfrac{\partial P}{\partial U_s} U_s \\ J_{Q\delta} = \dfrac{\partial Q}{\partial \delta}, \ J_{QU} = \dfrac{\partial Q}{\partial U_s} U_s \end{cases} \tag{19}$$

Where:

$$\begin{cases} P = P_s - P_{d1} - P_{d2} - P_{d3} \\ Q = Q_s + Q_{d1} - Q_{d2} - Q_{d3} - Q_c \end{cases} \tag{20}$$

Among them, P and Q are the active power and reactive power that cannot be offset in the AC bus.

From [16], when the active power at the converter bus remains unchanged, the relationship between the reactive power variable and voltage of the converter bus can be obtained by (18):

$$\begin{cases} \Delta Q = J_R \dfrac{\Delta U_s}{U_s} \\ J_R = J_{QU} - J_{Q\delta} J_{P\delta}^{-1} J_{PU} \end{cases} \tag{21}$$

In summary, the value of $\Delta Q/\Delta U_s$ in the multi-infeed system can be calculated by using (21), and then the value of DVSF can be obtained. Meanwhile, observation (21) shows that different control strategies adopted by the VSC-HVDC subsystem will have different effects on it. Therefore, the following will discuss the impact of different control strategies used by VSC-HVDC subsystem on DVSF.

A. VSC2 Uses Constant Reactive Power (CRP) Control / Constant DC Voltage (CDCV) Control, and VSC3 Uses Constant Active Power (CAP) Control

Under this scenario, the following relationships exist:

$$\begin{cases} \dfrac{\partial Q_{d2}}{\partial \delta} = \dfrac{\partial P_{d3}}{\partial \delta} = 0 \\ \dfrac{\partial Q_{d2}}{\partial U_s} U_s = \dfrac{\partial P_{d3}}{\partial U_s} U_s = 0 \end{cases} \tag{22}$$

Combining (1)-(6), (18), (19), and (22) can solve the elements in the Jacobian matrix:

$$\left\{ J_{P\delta} = \frac{U_s E(R_s \sin\delta - X_s \cos\delta)}{Z_s^2} + \frac{U_s U_c \cos(\delta_c - \delta)}{T_2 X_{T2}} \right. \tag{23}$$

$$\begin{cases} J_{PU} = \dfrac{2R_s U_s^2 - U_s E(R_s \cos\delta - X_s \sin\delta)}{Z_s^2} - \dfrac{6\sqrt{2}}{\pi T_1} U_s I_{d1} \cos\gamma \\ \quad - \dfrac{U_s U_c \sin(\delta_c - \delta)}{T_2 X_{T2}} \end{cases} \tag{24}$$

$$\left\{ J_{Q\delta} = \frac{U_s E(X_s \sin\delta - R_s \cos\delta)}{Z_s^2} - \frac{U_s U_c \sin(\delta_c - \delta)}{T_3 X_{T3}} \right. \tag{25}$$

$$\begin{cases} J_{QU} = \dfrac{2X_s U_s^2 - U_s E(R_s \sin\delta + X_s \cos\delta)}{Z_s^2} + \dfrac{6\sqrt{2} I_{d1} U_s (U_{d10} - U_{d1} \cos\gamma)}{\pi T_1 \sqrt{U_{d10}^2 - U_{d1}^2}} \\ \quad - \dfrac{T_3 U_s U_c \cos(\delta_c - \delta) - 2U_s^2}{T_3^2 X_{T3}} - 2B_c U_s^2 \end{cases} \tag{26}$$

B. VSC2 Uses CAP Control / CRP Control, and VSC3 Uses CDCV Control / Constant Bus Voltage (CBV) Control

Under this scenario, the following relationships exist:

$$\begin{cases} \dfrac{\partial P_{d2}}{\partial \delta} = \dfrac{\partial Q_{d2}}{\partial \delta} = 0 \\ \dfrac{\partial P_{d2}}{\partial U_s} U_s = \dfrac{\partial Q_{d2}}{\partial U_s} U_s = \dfrac{\partial P_{d3}}{\partial U_s} U_s = \dfrac{\partial Q_{d3}}{\partial U_s} U_s = 0 \end{cases} \tag{27}$$

Combining (1)-(6), (18), (19), and (27) can also solve the elements in the Jacobian matrix:

$$J_{P\delta} = \frac{U_s E(R_s \sin\delta - X_s \cos\delta)}{Z_s^2} + \frac{U_s U_c \cos(\delta_c - \delta)}{T_3 X_{T3}} \tag{28}$$

$$J_{PU} = \frac{2R_s U_s^2 - U_s E(R_s \cos\delta - X_s \sin\delta)}{Z_s^2} - \frac{6\sqrt{2}}{\pi T_1} U_s I_{d1} \cos\gamma \tag{29}$$

$$J_{Q\delta} = \frac{U_s E(X_s \sin\delta - R_s \cos\delta)}{Z_s^2} - \frac{U_s U_c \sin(\delta_c - \delta)}{T_3 X_{T3}} \tag{30}$$

$$J_{QU} = \frac{2X_s U_s^2 - U_s E(R_s \sin\delta + X_s \cos\delta)}{Z_s^2} + \frac{6\sqrt{2} I_{d1} U_s (U_{d10} - U_{d1} \cos\gamma)}{\pi T_1 \sqrt{U_{d10}^2 - U_{d1}^2}} - 2B_c U_s^2 \tag{31}$$

C. VSC2 Uses CAP Control / CBV Control, and VSC3 Uses CRP Control / CDCV Control

Under this occasion, the following relationships exist:

$$\begin{cases} \dfrac{\partial P_{d2}}{\partial \delta} = \dfrac{\partial P_{d2}}{\partial U_s} U_s = \dfrac{\partial Q_{d2}}{\partial U_s} U_s = 0 \\ \dfrac{\partial Q_{d3}}{\partial \delta} = \dfrac{\partial Q_{d3}}{\partial U_s} U_s = 0 \end{cases} \tag{32}$$

Observing (28), (30) and (31), we can see that only the value of J_{PU} is different at this situation, and the values of $J_{P\delta}$, $J_{Q\delta}$ and J_{QU} are the same as those in Chapter B. The solvable J_{PU} is shown below,

$$J_{PU} = \frac{2R_s U_s^2 - U_s E(R_s \cos\delta - X_s \sin\delta)}{Z_s^2} - \frac{6\sqrt{2}}{\pi T_1} U_s I_{d1} \cos\gamma - \frac{U_s U_c \sin(\delta_c - \delta)}{T_3 X_{T3}} \tag{33}$$

Fig.5 shows the relationship between the DVSF and the output power of the VSC-HVDC subsystem under the above three control modes drawn by Matlab software. Well known, the system impedance and the short-circuit ratio (SCR) show a reciprocal relationship according to the relevant references [21-22]. Meanwhile, it is generally considered that a system with SCR<2 is a weakest system, a system with 2<SCR<3 is a weak system, and a system with SCR>3 is a strong system.

Observing Fig.5, with the decrease of system impedance, the value of DVSF shows a clear upward trend. Especially when the system transitions from a weakest system to a strong system, the change of DVSF is very obvious, which further verifies that the voltage support capability of the LCC-HVDC subsystem is related to the system impedance. Observing

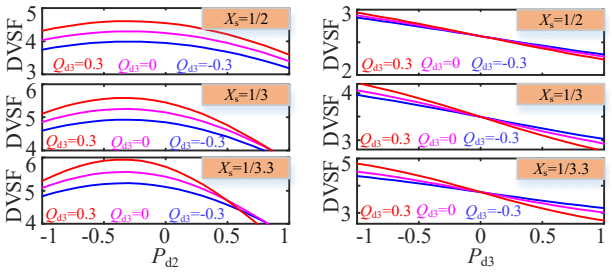

(a) (b)

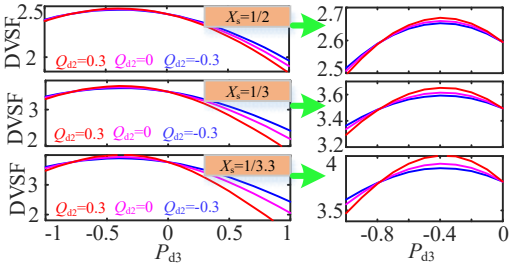

(c)

Fig. 5 The relationship between the power output by VSC-HVDC subsystem and DVSF under different control modes. (a). case A. (b). case B. (c). case C.

Fig. 5(a), when the control mode A is adopted, increasing the reactive power output by the VSC-HVDC subsystem can increase the value of DVSF, indicating that the voltage support capability-mVSCs-LCC is enhanced. When the active power output by the VSC-HVDC subsystem is increased, the value of DVSF reaches the maximum value at the negative active power, and then gradually decreases. Different from Fig.5(a), when control mode B is adopted in Fig.5(b), increasing the reactive power output by VSC-HVDC subsystem at the negative active power can improve the voltage support capability -mVSCs-LCC. On the contrary, at the positive active power, increasing the reactive power output by the VSC-HVDC subsystem can weaken it. In Fig.5(c), the voltage support ability of the control mode C to the LCC-HVDC at the positive active power is similar to that of the control mode B. However, unlike the control mode B, increasing the reactive power output by the VSC-HVDC subsystem at the negative active power in control mode C will cause the voltage support capability -mVSCs-LCC to first weaken and then enhanced.

In addition, comparing the three figures shows that the use of control mode A can enable the LCC-HVDC subsystem to obtain greater voltage support strength, and increasing the active power output of the system under the three control modes will reduce the voltage support capability -mVSCs-LCC as a whole.

IV. Validation

In order to verify the correctness of the evaluation indicators proposed in this paper, the simulation builds the multi-infeed HVDC system shown in Fig.2. The simulation parameters are shown in TABLE I. In the simulation, the output power of the VSC-HVDC subsystem was changed at 0.5s to explore its impact on the voltage support capability -mVSCs-LCC. The following three aspects will be verified in this paper: (1) The steady-state simulation waveform is used to verify the correctness of the model built in this paper. (2) The simulation waveform of DVSF is used to verify the rationality of its proposal. (3) The simulation waveforms of multiple VSC-HVDC subsystems with different control strategies are used to verify the voltage support capability of LCC-HVDC subsystems in weak AC grid.

TABLE I
SIMULATION PARAMETERS

Parameters	Values	Parameters	Values
E_s	1.1 p.u	X_{T1}, X_{T2}, X_{T3}	0.15 p.u, 0.15 p.u, 0.15 p.u

R_s	0	δ	90^0
X_s	0.269 p.u	T_1	220/150 kV
U_s	1 p.u	T_2	220/150 kV
Q_c	0.45 p.u	T_3	220/150 kV
γ	18°	B_c	0.45 p.u
θ	90°	δ_s	0^0
U_{d1}, U_{d2}, U_{d3}	300 kV(1 p.u)	I_{d1}, I_{d2}, I_{d3}	1 kA(1 p.u)

A. Validation of Steady-State Operating Models

In this paper, the hybrid multi-terminal HVDC system shown in Fig.2 is built in MATLAB/simulink software. Among them, the DC-side voltage is 300kV and the DC current fed into the three subsystems at the receiving-end grid is 1 kA. Fig.6 shows the DC voltage and current waveforms of the three subsystems at the receiving-end grid. As observed, the voltage and current waveforms in Fig.6 basically coincide because the rated values of the DC side voltage and current of the three receiving-end converter stations are set to be the same. In addition, the change trends of DC voltage and DC current are basically the same and both reach a steady state at about 0.2s, which also verifies the correctness of the simulation model. The difference between the two is that the harmonics of DC voltage are lower than that of DC current. The possible reason for this is that there is a constant DC voltage control in the receiving-end converter station, but there is a constant DC current control in the sending-end converter station. Therefore, this will cause the voltage waveform of the receiving-end converter station to be smoother than the current waveform.

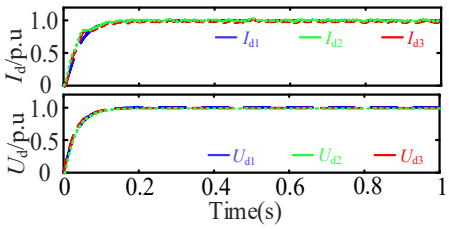

Fig. 6 DC-side voltage and current waveforms in steady state operation

B. Validation of DVSF

Fig.7 shows the simulation results using A, B, and C three control modes. As observed, with the decrease of system impedance (the increase of SCR), the value of DVSF under the three control modes shows an increasing trend, which indicates that the voltage support capability -mVSCs-LCC is enhanced. Meanwhile, when using control mode A, the reactive power output by the VSC-HVDC subsystem increases from -0.3 p.u to 0.3 p.u at 0.5s, which makes the DVSF value under different system impedances increase significantly. The above results indicate that increasing reactive power can improve the voltage support capability -mVSCs-LCC. However, difference from the simulation result obtained by using control mode A in Fig.7 (a) is that the reactive power of the system increases from -0.3 p.u to 0.3 p.u when the VSC-HVDC subsystem outputs positive active power in control mode B, the value of DVSF shows a decreasing trend, indicating that the voltage support capability -mVSCs-LCC is weakening. Similarly, different from the simulation results using control mode B in Fig.7 (b) is that the reactive power output by the VSC subsystem increases from -0.3 p.u to 0.3 p.u when the VSC-HVDC subsystem outputs negative active power in control mode C, the value of DVSF shows a trend of first decreasing and then increasing, indicating that the voltage support capability -mVSCs-LCC weakened first and then enhanced. The above time-domain simulation results based on MATLAB are basically consistent with the theoretical analysis in Fig.5. In addition, observing the three figures show that increasing the active power output by the VSC-HVDC subsystem can weaken the voltage support capability -mVSCs-LCC, and the use of control mode A can achieve higher voltage support capabilities than control modes B and C. TABLE II, TABLE III, and TABLE IV respectively give the simulation data under the above three control modes, which are basically consistent with the analysis results.

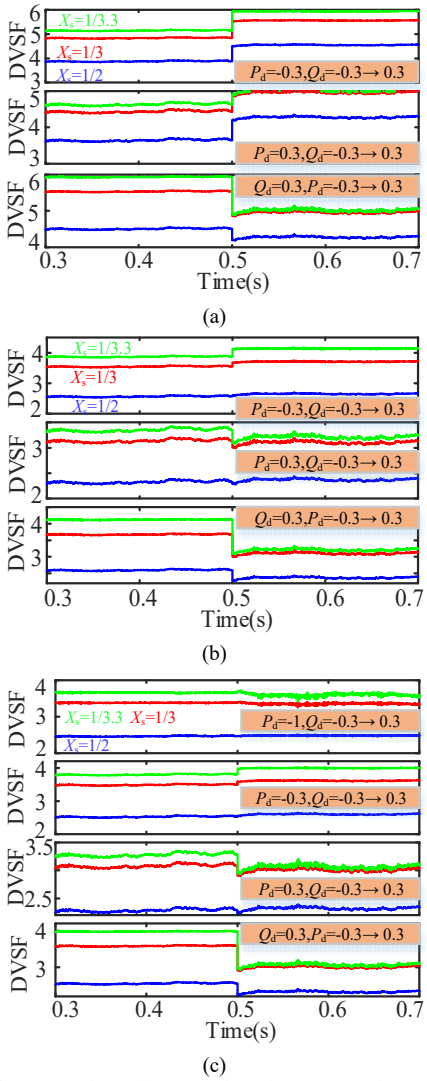

Fig. 7 Simulation results under control modes A, B, and C. (a). case A. (b). case B. (c). case C.

Since the receiving-end grid in other references only contains one VSC-HVDC subsystem, it does not reflect the coordinated control between the VSC-HVDC subsystems. Therefore, Fig.8 only shows the comparison of various evaluation indicators when the receiving-end power grid contains only one VSC-HVDC subsystem and adopts different

control strategies. As observed, no matter what control strategy the VSC-HVDC subsystem adopts, increasing its active power will decrease the value of the evaluation index. In order to verify whether the evaluation indicators proposed in this paper have such characteristics, TABLE V also gives the numerical values of the indicators proposed in this paper in three cases. It can be seen from TABLE V that with the increase of the output active power of the VSC-HVDC subsystem, the value of the DVSF also presents a downward trend. To sum up, DVSF can have the same evaluation function as other indicators.

TABLE II
SIMULATION RESULTS UNDER CASE A

Power change	DVSF		
	X_s=1/2	X_s=1/3	X_s=1/3.3
P_d=-0.3,Q_d=-0.3→0.3	3.878→4.504	4.84→5.53	5.15→5.933
P_d=0.3, Q_d=-0.3→0.3	3.638→4.2	4.428→4.898	4.626→4.925
Q_d=0.3, P_d=-0.3→0.3	4.504→4.192	3.684→4.864	5.935→4.898

TABLE III
SIMULATION RESULTS UNDER CASE B

Power change	DVSF		
	X_s=1/2	X_s=1/3	X_s=1/3.3
P_d=-0.3,Q_d=-0.3→0.3	2.56→2.595	3.545→3.676	3.871→4.127
P_d=0.3, Q_d=-0.3→0.3	2.335→2.289	3.15→3.002	3.353→3.092
Q_d=0.3, P_d=-0.3→0.3	2.595→2.283	3.684→3.008	4.127→3.099

TABLE IV
SIMULATION RESULTS UNDER CASE C

Power change	DVSF		
	X_s=1/2	X_s=1/3	X_s=1/3.3
P_d=-1,Q_d=-0.3→0.3	2.483→2.462	3.405→3.297	3.663→3.494
P_d=-0.3,Q_d=-0.3→0.3	2.528→2.566	3.487→3.581	3.797→3.98
P_d=0.3, Q_d=-0.3→0.3	2.289→2.239	3.087→2.91	3.277→2.945
Q_d=0.3, P_d=-0.3→0.3	2.551→2.239	3.588→2.907	3.982→2.945

TABLE V
COMPARISON OF DIFFERENT EVALUATION INDICATORS

References/Index	X_s=1/3, P_d=-0.3→0.3, Q_d=0		
Ref.[13]/AISCR	VSC uses CAP/CRP	VSC uses CAP/CBV	
	4.324→0.975	1.43→1.07	
Ref.[20]/CRVSF	VSC uses CAP/CRP	VSC uses CAP/CBV	
	1.075→0.752	3.067→2.843	
Ref.[23]/HGSCR	VSC uses CAP/CRP	VSC uses CAP/CBV	
	26.815→14.721	3.947→2.863	
This Paper/DVSF	VSC uses CAP/CRP	VSC uses CAP/CBV	
	3.513→2.933	3.412→2.861	
This Paper/DVSF	case A	case B	case C
	5.185→4.663	3.61→3.076	3.534→2.998

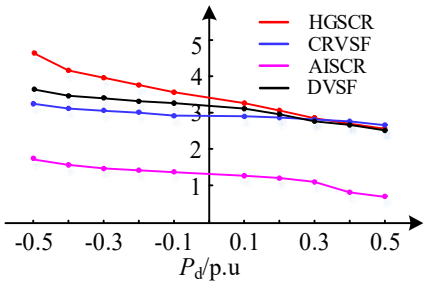

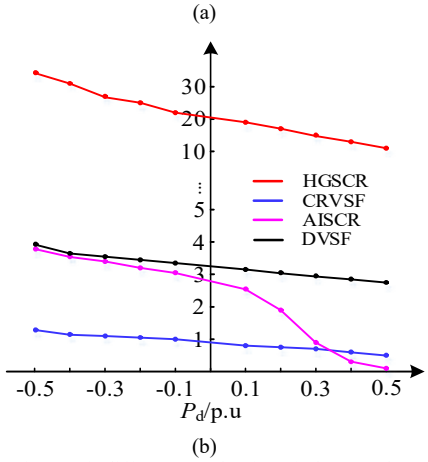

Fig. 8 Comparison of different evaluation indexes when VSC-HVDC system adopts different control strategies. (a). VSC uses CAP control / CBV control. (b). VSC uses CAP control / CRP control.

C. Validation of Multi-VSC-HVDC Subsystems Using Different Control Strategies

Fig.9 shows the *d*-axis component of the AC bus voltage in the case A, case B and case C when the voltage drop depth of the receiving-end grid is about 10%. As observed, the output voltages of control modes A, B and C are 0.9147 p.u, 0.8811 p.u, and 0.8678 p.u under this case, respectively. It is similar to the distribution order of the corresponding DVSF values in Table 2, Table 3 and Table 4. These data show that the voltage support capacity of control mode A is the largest, the voltage support capacity of control mode B is the second, and the voltage support capacity of control mode C is the lowest.

Fig.10 and Fig.11 show that the voltage drop depth of the receiving-end grid are about 30% and 55%, respectively. Observing them, in these two cases, the voltage support capability of control mode A is stronger than that of the other two control modes. Taking the voltage drop depth of 55% as an example, the output voltages in the three control modes are 0.5634 p.u, 0.5306 p.u and 0.5209 p.u in sequence. The above results also basically verify the correctness of the theory.

Fig.12 presents a situation where the voltage sag depth of the receiving-end grid is about 60%. As observed, unlike the above three simulation cases, the difference in voltage amplitudes output by the three control modes is not obvious at this situation, which indicates that only relying on the control strategy can not provide better voltage support for serious fault conditions.

D. Comparison of Advantages and Disadvantages of Different References

In order to let readers know the advantages and disadvantages of different references on the research of voltage support capability more clearly, TABLE VI gives a detailed comparison. Therefore, researchers can quickly find suitable research methods according to the advantages and disadvantages of each reference.

TABLE VI
COMPARISON OF DIFFERENT REFERENCES

Ref.	Advantage	Disadvantage

Ref.[13]	Analyzed the impact of the VSC operation strategy on the proposed indicators	There is no quantitative division of the strengths and weaknesses of the system.
Ref.[14]	The strength of the system is quantitatively divided.	The influence of VSC operation strategy on the proposed indicators is not considered
Ref.[17]	The impact of LCC and VSC operation strategies on the proposed indicators is considered.	There is no quantitative division of the strengths and weaknesses of the system.
Ref.[20]	The strength of the system is quantitatively divided.	The influence of VSC operation strategy on the proposed indicators is not considered.
Ref.[23]	Analyzed the impact of the VSC operation strategy on the proposed indicators	There is no quantitative division of the strengths and weaknesses of the system.
This paper	Quantitatively divide the strength of the system and consider the impact of the VSC operation strategy on the proposed indicators	The influence of LCC operation strategy and the electrical distance of the receiving-end grid on the proposed index is not considered.

V. CONCLUSION

This paper proposes a new index called dynamic voltage support strength factor (DVSF) to evaluate the voltage support capability -mVSCs-LCC in a hybrid multi-infeed system including weak AC grid. More meaningfully, this paper also analyzes the DVSF values of the VSC-HVDC subsystem with different control strategies in detail, which can provide a certain reference for the operation mode of the VSC-HVDC subsystem in the hybrid HVDC transmission project. Simulation and theoretical analysis can get different conclusions from other references as follows:

(1) When the VSC subsystem in control modes B and C outputs positive active power, increasing its reactive power can weaken the voltage support capability -mVSCs-LCC.

(2) When the VSC subsystem outputs negative active power in the control mode C, increasing its reactive power can make the voltage support capability -mVSCs-LCC weakened first and then enhanced.

(3) The use of constant reactive power control/constant DC voltage control for VSC2 and constant active power control for VSC3 enables the LCC subsystem to achieve higher voltage support capabilities.

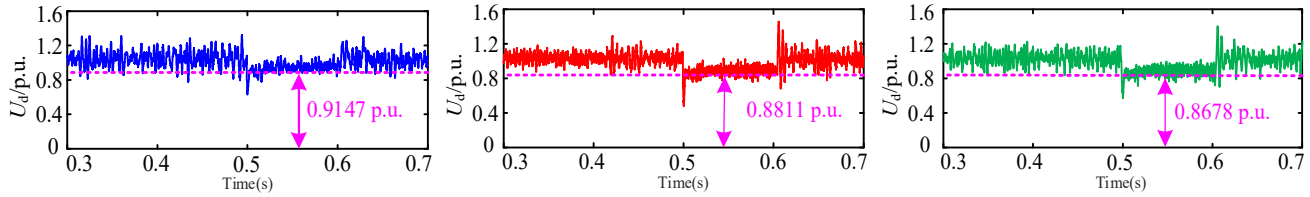

Fig. 9 The voltage of the receiving-end grid drops by about 10% when X_s=1/3. (a). VSC2 uses CRP/CDCV, and VSC3 uses CAP. (b). VSC2 uses CAP/CRP , and VSC3 uses CDCV/CBV. (c). VSC2 uses CAP/CBV , and VSC3 uses CRP/CDCV.

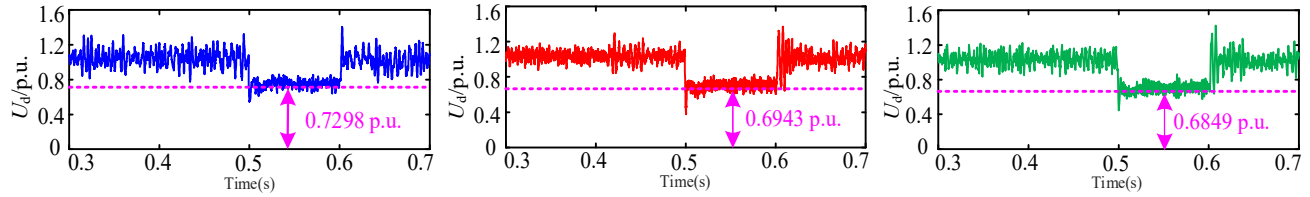

Fig. 10 The voltage of the receiving-end grid drops by about 30% when X_s=1/3. (a). VSC2 uses CRP/CDCV, and VSC3 uses CAP. (b). VSC2 uses CAP/CRP , and VSC3 uses CDCV/CBV. (c). VSC2 uses CAP/CBV , and VSC3 uses CRP/CDCV.

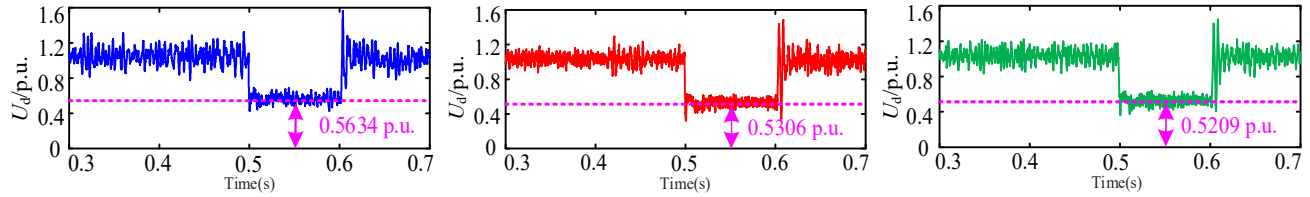

Fig. 11 The voltage of the receiving-end grid drops by about 55% when X_s=1/3. (a). VSC2 uses CRP/CDCV, and VSC3 uses CAP. (b). VSC2 uses CAP/CRP , and VSC3 uses CDCV/CBV. (c). VSC2 uses CAP/CBV , and VSC3 uses CRP/CDCV.

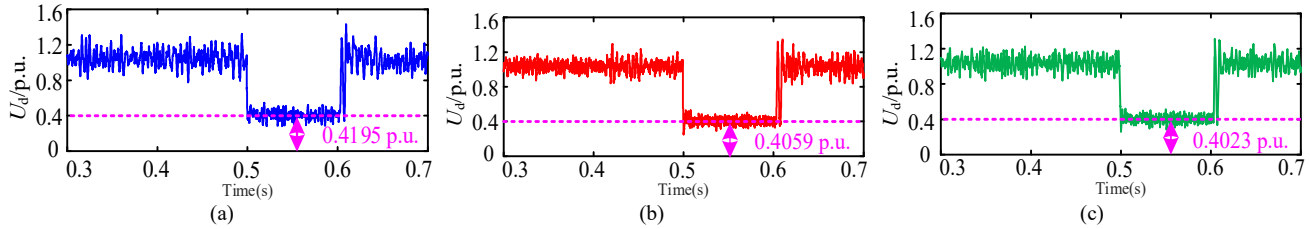

Fig. 12 The voltage of the receiving-end grid drops by about 60% when X_s=1/3. (a). VSC2 uses CRP/CDCV, and VSC3 uses CAP. (b). VSC2 uses CAP/CRP , and VSC3 uses CDCV/CBV. (c). VSC2 uses CAP/CBV , and VSC3 uses CRP/CDCV.

REFERENCES

[1] Li. Y.L, Zhang. Y.K., Song. J.Z., et al. "A novel pilot protection scheme for LCC-HVDC transmission lines based on smoothing-reactor voltage". *Electric Power Systems Research*, vol. 168, pp. 261-268, Mar. 2019.

[2] Kwon. DH, Kim. Y.J., and Moon. SI., "Modeling and Analysis of an LCC HVDC System Using DC Voltage Control to Improve Transient Response and Short-Term Power Transfer Capability", *IEEE Trans. Power Del.*, vol. 33, no. 4, pp. 1922-1933, Aug. 2018.

[3] Liu. Z.W, Miao. S.H, Fan. Z.H, et al. "Power Sliding Mode Compensation Strategy of VSC-HVDC under Unbalanced Grid Voltage ", *Transactions of China Electrotechnical Society*, vol. 33, no 14, pp. 3296-3305, Jul.2018.

[4] Sun. K.Q., Xiao. H.Q., Liu. S.Y., et al. "Machine Learning-based Fast Frequency Response Control for a VSC-HVDC System.", *CSEE J. Power Energy Syst*, vol. 7, no. 4, pp. 688-697, Jul. 2021.

[5] Shao. B.B. , Zhao. S.Q, Gao. B.F, et al. " Instability Mechanism and Criterion Analysis of VSC-HVDC Connected to the Weak AC Power Grid ". *Transactions of China Electrotechnical Society*, vol. 34, no 18, pp. 3884-3896, Sep.2019.

[6] Li. T., Li. Y.L, and Chen. X.L, et al. "Research on coordinated control strategy based on hybrid multi-terminal HVDC transmission network". *Int J Electric Power Energy Syst* , vol. 135, no. 107400, pp.1-11, Feb. 2022.

[7] Li. T., Li. Y.L, and Chen. X.L. "Fault Diagnosis with Wavelet Packet Transform and Principal Component Analysis for Multi-terminal Hybrid HVDC Network". *Journal of Modern Power Systems and Clean Energy*, vol. 9, no. 6, pp. 1312-1326, Dec. 2021.

[8] Wu. G.L., Liang. J., Zhou. X.X. et al. "Analysis and Design of Vector Control for VSC-HVDC Connected to Weak Grids". *CSEE J. Power Energy Syst*, vol. 3, no. 2, pp. 115-124, Jun. 2017.

[9] Chen. B.P., Lin. T., Chen. R.S, et al. " Characteristics of Multi-Band Oscillation for Direct Drive Wind Farm Interfaced with VSC-HVDC System ", *Transactions of China Electrotechnical Society*, vol. 33, pp. 176-184, Aug. 2018.

[10] Rehman. AU, Guo. C.Y, Zhao. C.Y. "AC system's strength evaluation of UHVDC system under hierarchical connection mode". *Electrical Engineering*, vol. 103, no. 4, pp. 2047-2056, Aug. 2021.

[11] Xiao. H, Li. Y.H, Zhu. J, et al. "Efficient approach to quantify commutation failure immunity levels in multi-infeed HVDC systems". *IET Gen Trans & Distr.*, vol. 10, no. 4, pp. 1032-1038, Mar. 2016.

[12] Ni. X.J, Aniruddha M. Gole, Zhao. C.Y, et al. "An Improved Measure of AC System Strength for Performance Analysis of Multi-Infeed HVdc Systems Including VSC and LCC Converters". *IEEE Trans. Power Del.*, vol. 33, no. 1, pp. 169-178, Feb. 2018.

[13] Guo. C.Y, Zhang. Y., Aniruddha M. Gole, et al. "Analysis of Dual-Infeed HVDC With LCC–HVDC and VSC–HVDC". *IEEE Trans. Power Del.*, vol. 27, no. 3, pp. 1529-1537, Jan. 2013.

[14] Xiao. H., Li. Y.H., and Sun. X.. "Strength Evaluation of Multi-Infeed LCC-HVDC Systems Based on the Virtual Impedance Concept". *IEEE Trans. Power Syst.*, vol. 35, no. 4, pp. 2863-2875, Jul. 2020.

[15] Xiao. H., Li. Y.H., Shi. D.Y., et al. "Evaluation of Strength Measure for Static Voltage Stability Analysis of Hybrid Multi-Infeed DC Systems". *IEEE Trans. Power Del.*, vol. 34, no.3, pp. 879-890, Jun. 2019.

[16] D. L. Hau Aik and Göran Andersson. "Analysis of Voltage and Power Interactions in Multi-Infeed HVDC Systems". *IEEE Trans. Power Del.*, vol. 28, no.2, pp. 816-824, Apr. 2013.

[17] Xiao. H. and Li. Y.H. "Multi-Infeed Voltage Interaction Factor: A Unified Measure of Inter-Inverter Interactions in Hybrid Multi-Infeed HVDC Systems". *IEEE Trans. Power Del.*, vol.35, no.4, pp.2040-2048, Aug. 2020.

[18] Jiang. M., Guo. Q.L, Sun. H.B., et al. "Short-Term Voltage Stability-Constrained Unit Commitment for Receiving-End Grid With Multi-Infeed HVDCs". *IEEE Trans. Power Syst.*, vol. 36, no. 3, pp. 2603-2613, May. 2021.

[19] D. L. Hau Aik and Göran Andersson. "Impact of Renewable Energy Sources on Steady-state Stability of Weak AC/DC Systems". *CSEE J. Power Energy Syst.*, vol. 3, no. 4, pp. 419-430, Dec. 2017.

[20] Xia. C.J., Li, X.P, Li. S.T., et al. "Definition and Analysis of Receiving System Voltage Support Strength Factor". *IEEE Access*, vol. 7: no. 134206-134214, Sep. 2019.

[21] Rokrok. E., Qoria. T., Bruyere. A., et al. "Classification and dynamic assessment of droop-based grid-forming control schemes: Application in HVDC systems". *Electric Power Systems Research*, vol. 189, no. 106765, pp. 1-7, Dec. 2020.

[22] Hoseinzadeh. B. and Frede. Blaabjerg. "Pre-design feasibility study of grid connected wind power plants under weak grid condition". *Electric Power Systems Research*, vol. 182, no. 106248, pp. 1-8, May. 2020.

[23] Li. D.D, Sun. M.X. and Fu. Y. "A General Steady-State Voltage Stability Analysis for Hybrid Multi-Infeed HVDC Systems", *IEEE Trans. Power Del.*, vol. 36, no. 3, pp. 1302-1312, Jun. 2021.

Tao Li (Student member, IEEE) received the B.Sc. and M.Sc. degrees in Shenyang Agricultural University and Shanghai University of Electric Power, China, in 2016 and 2019, respectively.

He is currently studying for a Ph.D with the School of Electrical and Information Engineering, Tianjin University. He is also serving as reviewer for different conferences and IEEE journal including *IEEE JESTPE*, *IEEE Access*, *IET Power Electronics*, *EPSR*, *ITEES*, *IEEE Trans. Circuits and Systems II* etc. His research interests include current-limiting, inverter control, HVDC, fault analysis, multilevel inverter, Z-source inverter, and so on.

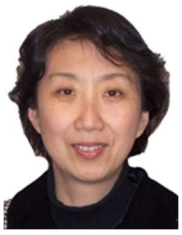

Yongli Li (Senior Member, CES) received the B.Sc. and M.Sc. degrees in electrical engineering from Tianjin University, China, in 1984 and 1987, respectively. In 1993, she received the Ph.D. degree in electrical engineering from the Universite Libre de Bruxelles, Belgium.

She is currently a Professor with the School of Electrical and Information Engineering, Tianjin University. Her research interests include fault analysis of power systems and fault diagnosis of electrical equipment, protection, and adaptive reclosing of EHV/UHV transmission systems, and protection and control of the microgrids, HVDC, and distribution networks.

Prof. Li is a member of CIGRE SC-B5.

Yuchen Zhu (Student member, IEEE) received the B.S. degree in electrical engineering from Tianjin University, Tianjin, China, in 2021, where he is currently working toward the Ph.D. degree. His research interests include MMC-HVDC, fault analysis and current limiting.